THE JOURNAL OF BIOLOGICAL CHEMISTRY VOL. 288, NO. 18, pp. 12667–12679, May 3, 2013

Function of Interfacial Prolines at the Transmitter-binding Sites of the Neuromuscular Acetylcholine Receptor*

Received for publication, December 10, 2012, and in revised form, March 15, 2013 Published, JBC Papers in Press, March 21, 2013, DOI 10.1074/jbc.M112.443911

Shaweta Gupta, Prasad Purohit, and Anthony Auerbach[1]

From the Department of Physiology and Biophysics, State University of New York at Buffalo, Buffalo, New York 14214

Background: Mutation of a proline at the AChR transmitter-binding site causes a congenital myasthenic syndrome.
Results: This proline interacts with a glycine across subunits but only when ACh is present.
Conclusion: Proline mutations impair the establishment of a high affinity for ACh, which requires a concerted inter-subunit backbone strain.
Significance: It is possible to engineer receptors having one functional binding site.

The neuromuscular acetylcholine (ACh) receptor has two conserved prolines in loop D of the complementary subunit at each of its two transmitter-binding sites (α-ϵ and α-δ). We used single-channel electrophysiology to estimate the energy changes caused by mutations of these prolines with regard to unliganded gating (ΔG_0) and the affinity change for ACh that increases the open channel probability (ΔG_B). The effects of mutations of ProD2 (ϵPro-121/δPro-123) were greater than those of its neighbor (ϵPro-120/δPro-122) and were greater at α-ϵ *versus* α-δ. The main consequence of the congenital myasthenic syndrome mutation ϵProD2-L was to impair the establishment of a high affinity for ACh and thus make ΔG_B less favorable. At both binding sites, most ProD2 mutations decreased constitutive activity (increased ΔG_0). LRYHQG and RL substitutions reduced substantially the net binding energy (made ΔG_B^{ACh} less favorable) by ≥2 kcal/mol at α-ϵ and α-δ, respectively. Mutant cycle analyses were used to estimate energy coupling between the two ProD2 residues and between each ProD2 and glycine residues (αGly-147 and αGly-153) on the primary (α subunit) side of each binding pocket. The distant binding site prolines interact weakly. ProD2 interacts strongly with αGly-147 but only at α-ϵ and only when ACh is present. The results suggest that in the low to-high affinity change there is a concerted inter-subunit strain in the backbones at ϵProD2 and αGly-147. It is possible to engineer receptors having a single functional binding site by using a α-ϵ or α-δ ProD2-R knock-out mutation. In adult-type ACh receptors, the energy from the affinity change for ACh is approximately the same at the two binding sites (approximately −5 kcal/mol).

Ion channels are molecular valves that regulate the flow of water and ions across cell membranes. In the mammalian central and peripheral nervous systems, neurotransmitters bind to synaptic receptor channels to increase the probability of channel opening and transmembrane currents. Agonists are small molecules that bind with a higher affinity to the O(pen) *versus* C(losed) channel conformational ensemble, so when these ligands occupy their target sites the C↔O "gating" equilibrium constant increases. We use the word gating to refer to the *entire* C↔O transition rather than just the conductance-changing microscopic step within the allosteric transition.

Acetylcholine (ACh),[2] the neurotransmitter at the vertebrate nerve-muscle synapse, has an ~6000-fold higher affinity for the O conformation of the adult-type muscle nicotinic acetylcholine receptor (AChR). Hence, ACh molecules at both of the two transmitter-binding sites increase the gating equilibrium constant by a factor of ~6000[2] (from $\sim 7 \times 10^{-7}$ to ~25). The amount of energy (kcal/mol) that each agonist molecule supplies to stabilize the O state is equal to −0.59 times the natural logarithm of the agonist affinity ratio. For adult wild-type mouse neuromuscular AChRs, the free energy from ACh at each site has been estimated to be $\Delta G_B^{ACh} = -5.1$ kcal/mol (1–3). This amount of energy from two binding sites is sufficient to overcome the +8.4 kcal/mol energy gap that separates C from O in the absence of agonists.

The neuromuscular AChR transmitter-binding sites are located in the extracellular domain of the protein at α-ϵ and α-δ subunit interfaces (Fig. 1*a*). These two sites are ~5 nm from each other and from a gate region in the transmembrane domain that regulates ionic conductance (4–6). There are conserved vicinal prolines at the binding sites in the complementary ϵ/δ subunit (ProD1 and ProD2; Fig. 1*b*). Fig. 1*c* shows some of the amino acids at the ligand-binding site of the *Lymnaea stagnalis* acetylcholine-binding protein, a soluble homolog of the AChR extracellular domain (7). The αC atoms of the residues corresponding to the AChR loop D prolines are shown as spheres (Pro-115 and Ser-116). Here, we report the functional consequences of mutations of the AChR prolines at both the α-ϵ and α-δ transmitter-binding sites, with regard to both the energy of unliganded gating (ΔG_0) and the energy from the affinity change for the transmitter (ΔG_B^{ACh}). The sum of these two quantities is equal to the energy difference between A_2O and A_2C (where A is the agonist), and it determines the diliganded gating equilibrium constant and the maximum open channel probability (see "Experimental Procedures").

* This work was supported, in whole or in part, by National Institutes of Health Grants NS-23513 and NS-064969.
[1] To whom correspondence should be addressed. Tel.: 716-829-3450; Fax: 716-829-2569; E-mail: auerbach@buffalo.edu.

[2] The abbreviations used are: ACh, acetylcholine; AChR, acetylcholine receptor; CMS, congenital myasthenic syndrome.

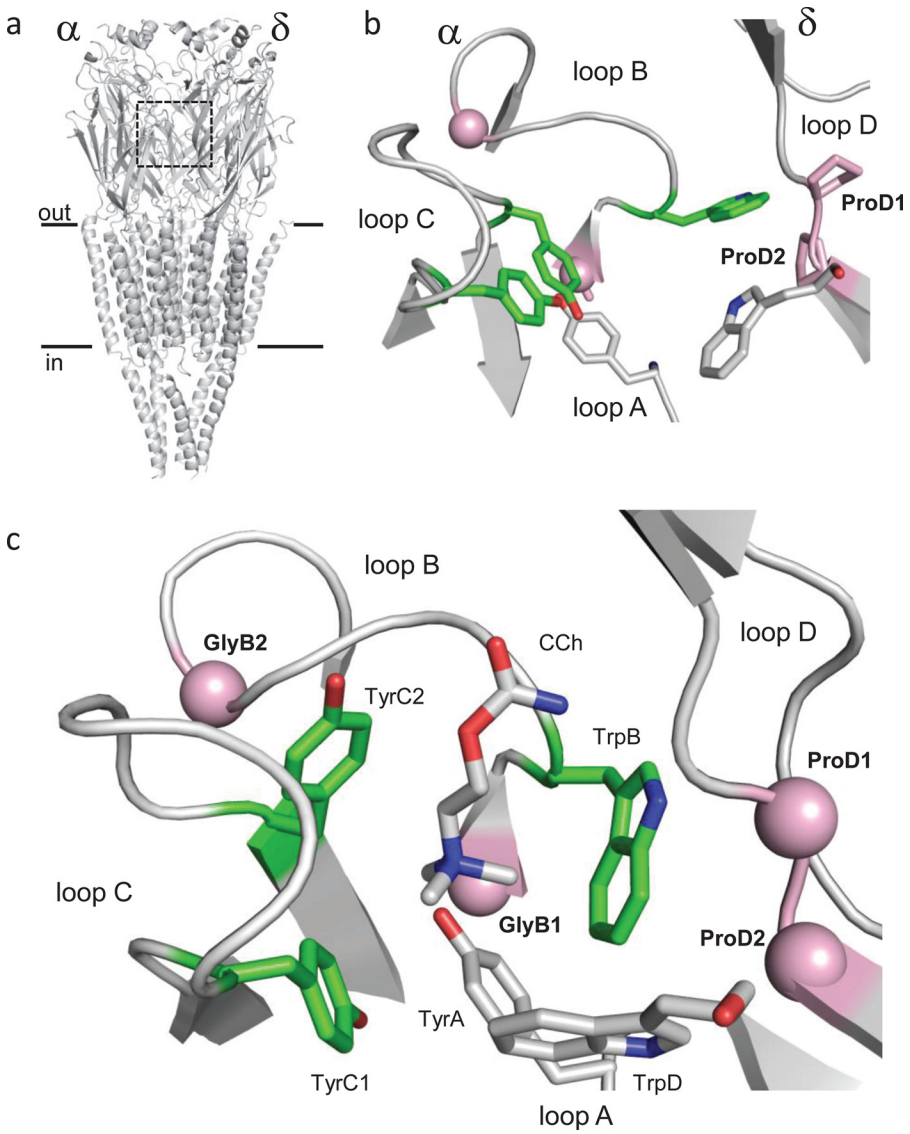

FIGURE 1. **Prolines at the AChR transmitter-binding site.** *a,* AChR has two transmitter-binding sites in the extracellular domain, at the α-ϵ and α-δ subunit interfaces (*boxed region*) (*Torpedo marmorata*; Protein Data Bank accession number 2bg9 (35)). *b,* unliganded *Torpedo* AChR α-δ transmitter-binding site. *Pink,* ProD1 and ProD2 on the complementary side of the binding site in loop D (*right*) and αC atoms of GlyB1 and GlyB2 in the α subunit (*left*). *Green,* energy from ACh binding is mainly from αTrp-149, αTyr-190, and αTyr-198. *c, L. stagnalis* acetylcholine-binding protein, ligand-binding site with carbamylcholine (*CCh*) (Protein Data Bank accession number 1uv6 (7)). The loop D αC atoms of Pro-115 and Ser-116 (*pink*) correspond to ProD1 and ProD2 in AChRs.

A leucine substitution at ϵProD2 causes a congenital myasthenic syndrome (CMS) and has been studied previously at the single-channel level in human AChRs (8). This mutation decreases the resting affinity of the α-ϵ transmitter-binding site by ~40-fold and the diliganded gating equilibrium constant by nearly 300-fold. The effects of leucine substitutions on whole-cell current dose-response curves have been measured in mouse AChRs, and a large right-shift was apparent, only for the ϵ subunit (ϵProD2-L) mutation (9).

The results are presented in five sections. 1) We describe a method to measure the change in ΔG_B^{ACh} caused by a ProD2 mutation at just one binding site. 2) The CMS mutation ϵProD2-L is analyzed according to a cyclic model of activation to estimate the high affinity equilibrium dissociation constant for ACh. 3) 25 different side chain substitutions of ProD2 at α-ϵ and α-δ are quantified with regard to their effects on ΔG_0 and ΔG_B^{ACh}. 4) Mutant cycle analyses reveal the degree of energy coupling between the two binding sites and between ProD2 and α subunit glycines at each binding site, both with and without ACh present. 5) We engineer AChRs to have a single functional binding site and estimate ΔG_B^{ACh} from α-ϵ and α-δ, independently.

EXPERIMENTAL PROCEDURES

Mutagenesis and Expression—Human embryonic kidney cells (HEK293) cells were maintained at 37 °C (95% air and 5% CO_2) and Dulbecco's minimum essential medium supplemented with 10% (v/v) fetal bovine serum plus 1% (v/v) penicillin/streptomycin (pH 7.4). The QuikChange site-directed mutagenesis kit (Stratagene) was used to introduce mutations in mouse AChR α, β, δ, and ϵ subunit cDNAs. All sequences were verified by dideoxy sequencing. The cells were transiently transfected with a mixture of cDNAs encoding WT or mutant subunits by calcium phosphate precipitation. 3.5–5 μg of DNA

per 35-mm culture dish, in the ratio of 2:1:1:1 ($\alpha/\beta/\epsilon/\delta$), and GFP (0.1 μg/μl, as a marker) were added for ~16 h. The cells were washed and electrophysiological recording commenced within 24–48 h.

Electrophysiology—Single-channel currents were recorded in the cell-attached patch configuration at 23 °C. Unless noted otherwise, the bath solution (K-PBS) (mM) contained the following: 142 KCl, 5.4 NaCl, 1.8 $CaCl_2$, 1.7 $MgCl_2$, 10 HEPES/KOH (pH 7.4). The pipette solution was always phosphate-buffered saline (PBS) (mM) and contained the following: 137 NaCl, 0.9 $CaCl_2$, 2.7 KCl, 1.5 KH_2PO_4, 0.5 $MgCl_2$, and 8.1 Na_2HPO_4 (pH 7.4). ACh was sometimes added but only to the pipette solution. For the measurement of diliganded currents, the pipette potential was held at −100 mV (which corresponds to a membrane potential of +100 mV) so that the single-channel currents were outward, and there was little or no channel block by ACh. For the measurement of unliganded currents (no channel block), the bath was PBS, and the pipette potential was held at +70 mV (which corresponds to a membrane potential of approximately −100 mV; inward currents). Patch pipettes were pulled from borosilicate capillaries to a resistance of ~10 megohms and coated with Sylgard (Dow Corning). Single-channel currents were recorded using a PC-505 amplifier (Warner instrument Corp., Hamden, CT) with low pass filtering at 20 kHz and digitized at a sampling frequency of 50 kHz using an SCB-68 data acquisition board (National Instruments).

Kinetic Analysis—QUB software was used to acquire and analyze the single-channel currents. Clusters of openings arising from the activity from a single AChR were selected by eye, and the currents were idealized into noise-free intervals (after digitally low pass filtering, 12 kHz) by using the segmental *k* means algorithm with a two-state C(losed)↔ O(pen) model (10) (starting rate constants, 100 s^{-1}). Rate constants were estimated from the idealized interval durations by using a maximum log-likelihood algorithm (11) after imposing a dead time correction (applied to both open and shut intervals) of 50 μs (12). In most of the diliganded experiments, the interval durations obtained at high [ACh] concentrations were fitted by the same two-state model, but in some cases another shut state was added to the model (connected to O) to accommodate a relatively rare and short lived (~2 ms) desensitized state. In ϵ/δProD2-GHY, an extra O state was added to accommodate an additional brief and relatively rare open component. In the unliganded experiments, an extra open state (connected to O) was added to the basic two-state scheme to accommodate a rate, long open component.

The energies arising from the affinity changes at the two binding sites were estimated by invoking a cyclic model for receptor activation (Fig. 2*a*) (4, 13–15). The rate and equilibrium constants for low affinity binding of ACh and the A_2C↔ A_2O transition were estimated using the kinetic scheme shown in Fig. 2*b*.

ΔG_0 Estimation—To increase the frequency and clustering of unliganded openings, three different background constructs were used as follows: α(D97A + Y127F + S269I) ("DYS"), αDYS + βL269D, and αDYS + β(L269D + T456F). αAsp-97 is in loop A; αTyr-127 is in strand β6; αSer-269 is near the C terminus of M2; βLeu-269 is in M2, and βThr-456 is in M4.

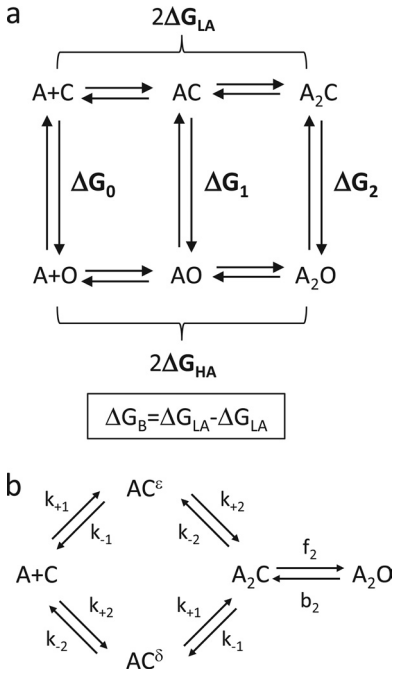

FIGURE 2. **State models.** *a*, thermodynamic cycle of the AChR activation. *A* is the agonist. The *vertical lines* are gating; *C* and *O* are the closed and open channel conformational ensembles. The *horizontal arrows* are binding; *C* is low affinity (*LA*) and *O* is high affinity (*HA*). The gating free energies, ΔG_n (where *n* is the number of bound agonists) are all $\Delta G_O - \Delta G_C$. The binding free energies, ΔG_{HA} and ΔG_{LA} are bound minus free for each of two equivalent sites. Without any external energy, the net energy change, C-to-A_2O, by clockwise and counterclockwise paths are equal, so $2\Delta G_{LA} + \Delta G_2 = \Delta G_0 + 2\Delta G_{HA}$. Rearranging and defining $\Delta G_B = \Delta G_{HA} - \Delta G_{LA}$ yields $2\Delta G_B = \Delta G_2 - \Delta G_0$. With unequal binding sites, $2\Delta G_B = \Delta G_{B1} + \Delta G_{B2}$ (see Equation 2). *b*, a two binding site scheme for AChR activation. The *superscripts* denote the α-ϵ or α-δ agonist-binding site. k_{+1} and k_{-1} are the α-ϵ agonist association/dissociation rate constants, and k_{+2} and k_{-1} are for the α-δ site ($K_d = k_-/k_+$). f_2 and b_2 are the diliganded forward and backward gating rate constants ($E_2 = f_2/b_2$).

Individually, each of these mutations only decreases ΔG_0 (is a gain-of-function) and has been shown not to affect either the resting equilibrium dissociation constant (K_d^{ACh}) or the free energy from binding (ΔG_B^{ACh}) (16–19). The $\Delta\Delta G_0$ values for each of these backgrounds are given in Table 1. Because there was no agonist in the pipette solution, there was no channel block; the inward single-channel current amplitude at −100 mV was ~7 pA. For each ProD2 mutation + background, the unliganded forward (f_0) and backward (b_0) gating rate constants were measured from the single-channel current interval durations, and their ratios were computed to give E_0^{obs}. $\Delta\Delta G_0$ for the ProD2 mutation alone (kcal/mol) was calculated as $-0.59\ \ln(E_0^{obs}/E_0^{bkg})$.

For example, for the ϵProD2-A, the observed values were $f_0/b_0 = 102\ s^{-1}/5818\ s^{-1} = 0.018$ (Table 3), obtained using the B2 background (αDYS + βL269D) (see Table 1). E_0 for just the background was 0.19 (Table 1), so $\Delta\Delta G_0^{\epsilon ProD2\text{-}A} = -0.59\ \ln(0.018/0.19) = +1.4$ kcal/mol. Table 3 shows $\Delta\Delta G_0$ values for all of the ProD2 mutants. In Fig. 4, these energy differences have been added to the WT unliganded gating free energy (+8.4 kcal/mol (2)) to give a ΔG_0 value for the mutant construct.

The net ΔG_0 of AChRs having all three perturbations (voltage, background mutation(s), and a ProD2 mutation) was calculated using Equation 1,

$$\Delta G_0^{net} = \Delta G_0^{wt} + \Delta\Delta G_0^{volt} + \Delta\Delta G_0^{bkg} + \Delta\Delta G_0^{Pro\text{-}mut} \quad \text{(Eq. 1)}$$

ΔG_B^{ACh} *Estimation*—At low agonist concentrations, the interval durations within clusters reflect both binding and gating. To estimate E_2, high [ACh] was used to eliminate delays associated with agonist binding. The membrane potential was held at +100 mV to reduce channel block. Depolarization from −100 to +100 mV decreases E_0 by ~12.5-fold or $\Delta\Delta G_0^{+200\ mV}$ = +1.5 kcal/mol (1). To compensate for the effect of depolarization on gating, and to place the experimental rate constants into a range that is easily measured by the patch clamp, we added background mutation(s) (1). The $\Delta\Delta G_0$ values for these background mutations are given in Table 1. We assumed that the voltage and background mutations were energetically independent. The diliganded opening (f_2) and closing rate constants (b_2) of the construct were measured using either 30 mM ACh (~180 times larger than K_d^{WT}) or 100 mM ACh. The cluster P_o did not change with this increase in [ACh], signifying that the binding delays had been eliminated. Using the observed rate constant, we calculated $E_2 = f_2/b_2$, and ΔG_2^{ACh} (kcal/mol) = $-0.59 \ln E_2$ (Table 4).

The difference in binding energy, higher *versus* lower affinity, is an energy source that increases the channel open probability. We call this energy difference at each transmitter-binding site ΔG_{B1} (α-ϵ site) and ΔG_{B2} (α-δ site). From detailed balance, we get Equation 2,

$$\Delta G_{B1} + \Delta G_{B2} = \Delta G_2 - \Delta G_0 \quad \text{(Eq. 2)}$$

In the experiments described below, ACh was the only agonist used to activate the AChRs. Studies of mono-liganded gating indicate that in WT adult mouse AChRs, the energy from the neurotransmitter is approximately −5.1 kcal/mol at each site ($\Delta G_{B1}^{ACh} \approx \Delta G_{B2}^{ACh}$) (20). In AChRs having a substitution of just one ProD2 (at either α-ϵ or α-δ), the energy from the affinity change at the mutated binding site is as shown in Equation 3,

$$\Delta G_B^{ACh,mut} = \Delta G_2^{ACh} - \Delta G_0^{net} + 5.1 \quad \text{(Eq. 3)}$$

For example, for the ϵProD-R mutation, the measured f_2/b_2 was 211 s^{-1}/4175 s^{-1}, or E_2^{obs} = 0.05 (+100 mV, αC418Y background; Table 4). Taking the natural log and multiplying by −0.59, we calculate ΔG_2^{ACh} = +1.8 kcal/mol. The ΔG_0^{net} (Equation 1) for this background was +8.4(WT) + 1.5(+100 mV) − 2.5(αC418Y) + 1.4(ProD2-R; Table 3) = +8.8 kcal/mol. From Equation 3, for ϵProD2-R ΔG_B^{ACh} = 1.8 − 8.8 + 5.1 = −1.9 kcal/mol (Table 4).

Error Estimates—The error limits for E_0 and E_2 are given in Tables 3 and 4 and were calculated from the forward/backward rate constant ratio measured for each patch. The errors in ΔG were estimated as $s_{\Delta_G} = 0.59(s_E/E)^2$, where s_E is the S.E. of the equilibrium constant. We then estimated the error in ΔG_0^{net} (Equation 1) as $s_{\Delta_G}0net = \sqrt{((s_{\Delta_G}0WT)^2 + (s_{\Delta\Delta G0Pro\text{-}mut})^2)}$ using $s_{\Delta_G}0WT$ = 0.2 kcal/mol (2). We did not have an estimate for the error associated with depolarization, so we assumed it to be negligible. $\Delta G_B^{ACh,\ WT} = -5.1 + 0.02$ kcal/mol (1), so total error associated with $\Delta G_B^{ACh,\ mut}$ is $s\Delta G_B = \sqrt{((s_{\Delta_G}2WT)^2 + (s_{\Delta_G}0net)^2 + (0.02)^2)}$ (see Equation 3). These errors are shown for each mutant in Table 4.

Coupling Energy Estimation—ΔG_0 and ΔG_B^{ACh} were estimated for single- and double-mutant constructs, as described above. For unliganded gating, the coupling free energy was estimated as ΔG_0(observed) − ΔG_0(predicted), where ΔG_0(predicted) is the sum of the ΔG_0 values of each mutation alone.

For example, for the ϵProD-S and αGlyB1-S combination E_0 = 0.016 (Table 5), so ΔG_0 = +2.4 kcal/mol. This result was obtained using the B13 background (ΔG_0 = −0.3 kcal/mol; Table 1), so the mutation-only ΔG_0(observed) = +2.4 −(−0.3) = +2.7 kcal/mol. The ΔG_0 values for each mutation alone were +1.2 kcal/mol (Table 3) and +2.2 kcal/mol (21); hence, ΔG_0(predicted) = +3.4 kcal/mol. Thus, coupling free energy for unliganded gating in the ϵProD-S + αGlyB1-S pair was 2.7–3.4 = −0.7 kcal/mol (Table 5).

To calculate the ΔG_B coupling energy for the ϵ/δProD2 and αGlyB pairs, we first estimated the observed total energy from ACh at two binding sites as shown in Equation 4,

$$\Delta G_B^{obs} = \Delta G_{B1} + \Delta G_{B2} = \Delta G_2^{ACh} - \Delta G_0^{net} \quad \text{(Eq. 4)}$$

The predicted total ΔG_B^{ACh} energy is the sum of the energies from the two binding sites. One of the binding sites had only the αGlyB mutation, and this energy is known (21), ΔG_{B2}^{GlyB}. The other binding site had both the ProD2 mutation and the αGlyB mutation, with $\Delta\Delta G_B^{ACh}$ values for each having been measured separately. Assuming independence, we achieve Equation 5,

$$\Delta G_B^{pred} = \Delta G_{B1}^{wt} + \Delta\Delta G_{B1}^{ProD2} + \Delta\Delta G_{B1}^{GlyB} + \Delta G_{B2}^{GlyB} \quad \text{(Eq. 5)}$$

For example, for the same mutant pair discussed above, E_2^{ACh} = 0.005 or ΔG_2^{ACh} = +3.1 kcal/mol (Table 6). This was obtained using the B5 + B0 background, so the net ΔG_0 (Equation 1) was +8.4(WT) + 1.5 (+100 mV) − 5.2(αY127F + αS269I) + 2.7(double mutant) = +7.4 kcal/mol (Table 6). The observed total energy from ACh at two binding sites (Equation 4) was −4.4 kcal/mol. The predicted total energy (Equation 5) was −5.1(WT) −0.4(ϵProD2-S) + 1.7(αGlyB1-S) − 3.3(αGlyB1-S) = −7.1 kcal/mol (Table 6). We can now compute the ΔG_B^{ACh} coupling free energy for the ϵProD-S and GlyB1S pair as −4.4−(−7.1) = +2.7 kcal/mol. We assume that the coupling energy is between the GlyB1 residue that is close to the mutated ProD2 residue, rather than the GlyB2 residue at the other transmitter-binding site.

K_d *Estimation*—The low affinity ACh association (k_{on}) and dissociation (k_{off}) rate constants for ϵProD2-L were estimated by fitting globally intra-cluster open and shut interval durations obtained at three different ACh concentrations (Fig. 3*d*). Because the leucine substitution influences only the α-ϵ-binding site, a model having two nonequivalent binding sites was used to fit the interval durations (Fig. 2*b*). The background mutation was αC418Y (in αM4), and the membrane potential was +100 mV. f_2 was fixed to the value determined at 30 mM ACh, and one association and the corresponding dissociation rate constant were fixed to the wild-type values. Three free

parameters were optimized as follows: k_+, k_-, and b_2 (Table 2). The K_d value was calculated as the ratio k_-/k_+.

One-site AChRs—The apparent forward rate constant (f_1) and an apparent backward (b_1) rate constant were quantified in AChRs having only one functional binding, using 500 μM ACh, −100 mV, and either of two different background mutations (αS269I and αP272A). Because the WT-binding site was not saturated at this [ACh], f_1 was less than the true opening rate constant by the factor $([ACh]/K_d)/(1 + [ACh]/K_d) = 0.75$ (K_d = 166 μM). Likewise, b_1 was less than the true channel closing rate constant because of channel block by the factor $1/(1 + [ACh]/K_B)$, where K_B is the equilibrium dissociation constant for channel block by ACh (~1.2 mM at −100 mV). These two effects cancel, so $E_2^{ACh,\,-100\,mV} = f_1/b_1$, and $\Delta G_1^{ACh} = -0.59 \ln(E_1) - \Delta\Delta G_0^{bkg}$ (Table 7).

RESULTS

Energy Measurements—In neuromuscular AChRs, desensitization is much slower than binding and gating, so in steady-state, single-channel recordings, openings occur in isolated clusters that are generated by the activity of just one AChR (Fig. 3*a*). The rate constants for agonist binding and $A_2C \leftrightarrow A_2O$ gating were estimated from the durations of intervals within clusters at different [ACh]. The opening/closing rate constant ratio is the gating equilibrium constant, which we measured both in the absence (E_0) or presence of ACh at one (E_1) or both (E_2) transmitter-binding sites. The natural logs of these experimentally determined constants are proportional to the free energy differences, O *versus* C, in a receptor having zero (ΔG_0), one (ΔG_1^{ACh}), or two (ΔG_2^{ACh}) bound ACh molecules.

The measured equilibrium constants and calculated energies pertain to the *full isomerization* of the AChR and not just the molecular rearrangements of the gate region that regulate ionic conductance. There are brief intermediate states between C and O (22, 23). We did not detect these directly, so the gating equilibrium constants (energies) we report are the products (sums) of those connecting these intermediates. For example, if the expanded gating model is $C \leftrightarrow F \leftrightarrow O$ (where F is an undetected intermediate), then the E_0 value we measure is the product of the $C \leftrightarrow F$ and $F \leftrightarrow O$ equilibrium constants, and the ΔG_0 value is the sum of the energy changes for the two steps.

ΔG_0 is the intrinsic free energy difference between the C and O ground states when there is only water at the binding sites (= $-0.59 \ln E_0$). Ignoring desensitization, this energy sets the minimum cluster open probability (P_o), which pertains to activity in the complete absence of agonists. ΔG_2^{ACh} is the free energy difference between the ground states when ACh is present at both sites (= $-0.59 \ln E_2$). This energy sets the maximum P_o. In WT AChRs under a reference condition (−100 mV, 23 °C), ΔG_0 = +8.4 kcal/mol and ΔG_2^{ACh} = −1.9 kcal/mol, with minimum and maximum P_o values of ~0.0000007 and ~0.96.

In brief, we measure E_0 and E_2^{ACh} for each mutant and take the logs to compute ΔG_0 and ΔG_2^{ACh}. We then use Equation 3 to estimate ΔG_B^{ACh} at the single mutated binding site. Measuring E_0 is an essential part of the process because mutations of binding site residues can have a significant effect on unliganded gating (24).

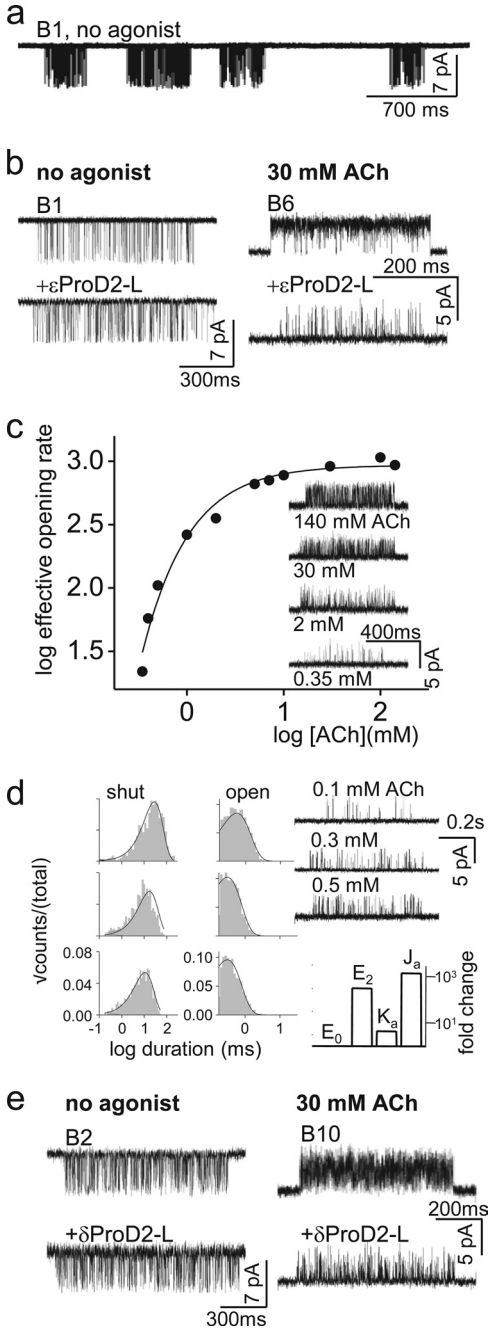

FIGURE 3. **CMS mutation ϵProD2-L.** *a,* unliganded openings (no agonist) at low time resolution (−100 mV). Each cluster of openings (downward; displayed at 2 kHz filtering) arises from the activity of one AChR. Silent periods between clusters are when all AChRs in the patch are desensitized. *B1* is the background (Table 1). *b,* ϵProD2-L had no effect on cluster P_o in the absence of agonists (*left,* −100 mV) but a large inhibitory effect on diliganded gating (*right,* +100 mV). *c,* with ϵProD2-L, the effective opening rate asymptotes at ~30 mM ACh, signifying saturation of the binding sites (+100 mV, background B8; *inset*, example clusters). *d, left,* interval duration histograms (background, B9). *Solid lines* calculated from the rate constants estimated by a global cross-concentration fit by the two binding site scheme (Table 2). *Right, top,* example of single-channel currents at different [ACh]. *Bottom,* fold-changes in the binding and gating equilibrium constants (WT/mutant) as follows: E_0, E_2, unliganded, and diliganded gating equilibrium constants; K_a, J_a, low and high affinity equilibrium *association* constants. *e,* example clusters from AChRs with a ProD2-L substitution in the δ subunit. There was little effect on unliganded gating (*left,* −100 mV) and a smaller effect on diliganded gating (*right,* +100 mV) compared with the ϵ subunit (see *b*). For all panels, background constructs are given in Table 1.

TABLE 1

Background constructs

bkg means background notation; E^{app} means apparent equilibrium constant of the background (* indicates calculated assuming energetic independence of each mutation; all others measured experimentally); $\Delta\Delta G_0$, relative free energy $= -0.59 \ln(E^{app}/E^{DYS, cho, or ACh})$, where $E_0^{DYS} = 0.047$, $E_2^{cho} = 0.046$, and $E_2^{ACh} = 25.4$.

Bkg	Ligand	Construct	E^{app}	$\Delta\Delta G_0$	Ref.
B0		+100 mV		1.5	1
B1	None	DYS	0.047		3
B2	None	DYS + βL269D	0.194	−0.8	
B3	None	DYS + β(L269D + T456F)	1.455	−2.0	
B4	None	DYS + αN217K + βT464F	11.24*	−3.2	
B5	None	α(Y127F + S269I)	0.0003*	−5.2	
B6	None	α(D97A + S269I)	0.0008*	−5.8	
B7	cho	αV283W	1.28	−1.4	25
B8	cho	αP272A	10.9	−3.2	30
B9	cho	αC418Y	7.84	−2.5	17
B10	cho	βT464F	0.57	−1.0	17
B11	ACh	α(P272G + V283W), +100 mV	0.77	2.1	
B12	ACh	α(Y127C + P272G + V283W),+ 100 mV	0.0042*	5.1	
B13	None	DYS + δV269C	1.65	−2.1	3
B14	None	DYS + εV265M	1.77	−2.1	3

To estimate E_0 and E_2^{ACh}, it was necessary to use background mutations and depolarization to place the gating rate constants into a measurable range (Table 1). These perturbations, alone or in combination, only changed ΔG_0 and had no effect on ΔG_B^{ACh}. An example analysis is provided below.

Leucine Substitutions—Fig. 3*b* shows unliganded and diliganded single-channel current clusters from AChRs having a εProD2-L substitution, the CMS mutation. The unliganded currents were recorded at a membrane potential of −100 mV, with the εProD2-L mutation expressed on a background construct that increased constitutive activity exclusively by reducing (making less positive) ΔG_0. The E_0 of unliganded clusters was approximately the same with or without the ProD2-L mutation (Table 2). This indicates that the Leu substitution did not change ΔG_0. The effect of the εProD2 mutant on gating without agonists was $\Delta\Delta G_0^{ProD2\text{-}L} = +0.0$ kcal/mol (Table 3).

Diliganded currents (30 mM ACh) were recorded at +100 mV to reduce channel block by the agonist. Relative to −100 mV, this depolarization increases the intrinsic energy of gating by $\Delta\Delta G_0^{+200\ mV} = +1.5$ kcal/mol (1). Depolarization shortens the open channel lifetime making it difficult to estimate accurately the channel closing rate constant, so we added a background mutation (αV283W, in M3) that slowed independently the closing rate constant. This background mutation increases E_0 by ~10-fold ($\Delta\Delta G_0^{\alpha V283W} = -1.4$ kcal/mol) (25). ΔG_B^{ACh} at either binding site was not altered by voltage or the αM3 background mutation. From Equation 1, $\Delta G_0^{net} = +8.5$ kcal/mol. E_2^{ACh} for this construct was estimated from the ratio of the forward/backward isomerization rate constants at 30 mM ACh, a concentration that fully saturates the transmitter-binding sites (Fig. 3*c*). The results were: $326\ s^{-1}/4639\ s^{-1} = 0.07$ (Table 2). Taking the log, we estimate that for this construct $\Delta G_2^{ACh} = +1.5$ kcal/mol. Because we had estimates for both ΔG_0^{net} and ΔG_2^{ACh}, we could compute for the CMS mutant $\Delta G_B^{ACh} = -1.9$ kcal/mol (Equation 3; Table 4). We conclude that the CMS mutation reduces the energy from the neurotransmitter at the α-ε site by ~63% (from −5.1 to −1.9 kcal/mol), or $\Delta\Delta G_{B1}^{ProD2\text{-}L} = +3.2$ kcal/mol.

We also measured the ACh equilibrium dissociation constant for the resting low affinity conformation of the binding site (K_d^{ACh}) by fitting intra-cluster current interval durations across several different concentrations (Fig. 3*d*). K_d^{ACh} was calculated from the dissociation/association rate constant ratio (Table 2). The result was $K_d^{ACh, ProD2\text{-}L} \approx 510\ \mu M$, which is only ~3 times larger than at the WT α-ε-binding site (16, 26). Based on cluster frequency and duration, there was no qualitative effect of the εProD-L mutation on desensitization, either with or without ACh at the transmitter-binding sites.

TABLE 2

Rate and equilibrium constants for wt and εProD2-L (ACh)

The abbreviations used are as follows: f_0, unliganded opening rate constant; b_0, unliganded closing rate constant; E_0, unliganded gating equilibrium constant ($= f_0/b_0$); f_2, diliganded opening rate constant; b_2, diliganded closing rate constant; E_2, diliganded gating equilibrium constant ($= f_2/b_2$); k_+, low affinity ACh association rate constant; k_-, low affinity ACh dissociation rate constant; K_d, low affinity equilibrium dissociation constant ($= k_-/k_+$); J_d, calculated high affinity equilibrium dissociation constant. Values estimated by cross-concentration fitting (mean ± S.D.): 100, 200, and 500 μM (one patch at each [ACh]; 16,400 intervals total). WT values are from Ref. 3 (f_0, b_0, and E_0), Ref. 1 (f_2, b_2, and E_2), and Ref. 26 (k_+, k_-, and K_d).

	WT	εProD2-L
f_0^a (s^{-1})	187	229 ± 17
b_0^a (s^{-1})	3994	5068 ± 284
E_0^a	0.047	0.046 ± 0.004
f_2^b (s^{-1})	65,850	245 ± 22
b_2^b (s^{-1})	2595	2962 ± 268
E_2^b	25.4	0.08 ± 0.008
k_+ ($\mu M^{-1}s^{-1}$)	106	6.0 ± 1.5
k_- (s^{-1})	17,614	3049 ± 775
K_d (μM)	166	508 ± 181
J_d(μM)	0.028	27-
K_d/J_d	6024	19-

[a] The observed values used the DYS background.
[b] The WT values are after correction for the background mutation (αV283W) and depolarization.

Fig. 3*e* shows the effects of a Leu substitution at the α-δ-binding site (δProD2-L). Unliganded gating was unaffected ($\Delta\Delta G_0 = 0.0$ kcal/mol), and the binding energy from ACh was reduced only by ~37% ($\Delta\Delta G_B = +1.9$ kcal/mol), which is about half of the effect of this mutation at the α-ε site (Table 4).

We also investigated the effects of a Leu substitution at ProD1 in the ε or δ subunit, but only with regard to the diliganded gating equilibrium constant E_2^{ACh} (Table 4). In both subunits, the reduction in E_2 was much smaller at ProD1 compared with ProD2.

Other Mutations—We examined other side chain substitutions at the ProD2 position in the ε and δ subunits. The ΔG_0 values for each binding site mutation are shown in Fig. 4*a* (Table 3). All of the mutations except for Leu made ΔG_0 more positive (reduced constitutive activity). In ε, the largest changes

TABLE 3

Effect of ϵ/δProD2 mutations on unliganded gating rate and equilibrium constants

The abbreviations used are as follows: bkg, background (see Table 1); f_0, observed unliganded opening rate constant (all rate constants are s^{-1}); b_0, observed unliganded closing rate constant; E_0, observed unliganded gating equilibrium constant ($= f_0/b_0$). Values are mean ± S.E., *n* patches. $\Delta\Delta G_0$, unliganded gating free energy change, kcal/mol ($= -0.59 \ln E_0^{obs}/E_0^{bkg}$). All non-zero values are positive, indicating that these mutations reduced constitutive activity.

		Observed				
Mutant	bkg	f_0	b_0	E_0	$\Delta\Delta G_0$	*n*
ϵProD2-L	B1	229 ± 17	5068 ± 284	0.045 ± 4.0E-03	0.0	5
-Y	B1	69 ± 9	3100 ± 620	0.022 ± 2.0E-04	0.4	3
-Q	B1	32 ± 7	3481 ± 451	0.009 ± 1.1E-03	1.0	3
-C	B2	95 ± 8	2819 ± 307	0.034 ± 4.0E-03	1.1	5
-V	B2	75 ± 6	2392 ± 272	0.031 ± 4.0E-03	1.1	5
-T	B1	18 ± 5	2878 ± 488	0.006 ± 8.0E-04	1.2	3
-H	B3	174 ± 32	1136 ± 83	0.153 ± 4.2E-02	1.3	3
-R	B2	66 ± 11	3859 ± 175	0.017 ± 3.5E-03	1.4	4
-K	B3	109 ± 7	2581 ± 108	0.042 ± 4.3E-03	2.1	5
-G	B3	123 ± 6	3258 ± 109	0.038 ± 1.7E-03	2.2	4
-S	B3	72 ± 13	2231 ± 238	0.032 ± 1.0E-02	2.2	3
-A	B2	102 ± 30	5818 ± 1093	0.018 ± 6.0E-03	1.4	3
δProD2-L	B2	265 ± 65	1359 ± 206	0.195 ± 1.7E-02	0.0	3
-K	B1	155 ± 17	4330 ± 289	0.036 ± 6.0E-03	0.2	5
-A	B2	168 ± 72	4945 ± 1669	0.034 ± 8.4E-02	1.0	3
-V	B3	327 ± 13	855.3 ± 68	0.382 ± 4.3E-02	0.8	3
-R	B2	123 ± 31	2766 ± 169	0.044 ± 1.4E-02	0.9	3
-S	B3	236 ± 10	1240 ± 118	0.190 ± 1.9E-02	1.2	3
-Y	B2	34 ± 3	2164 ± 455	0.016 ± 4.1E-02	1.5	3
-C	B2	37 ± 1	2313 ± 202	0.016 ± 1.8E-03	1.5	2
-G	B3	41 ± 11	371.3 ± 129	0.110 ± 6.9E-02	1.5	3
-H	B3	70 ± 24	718 ± 57	0.097 ± 4.3E-02	1.6	3
-D	B3	63 ± 15	1325 ± 50	0.048 ± 1.0E-02	2.0	3
-T	B3	172 ± 26	4191 ± 438	0.041 ± 3.0E-03	2.1	6
-Q	B3	40 ± 3	1821 ± 57	0.022 ± 1.0E-03	2.5	3

TABLE 4

Effect of ϵ/δProD1 and ProD2 mutations on diliganded gating rate and equilibrium constants and ΔG_B^{Ach}

The abbreviations are as follows: bkg, background (see Table 1); f_2, diliganded opening rate constant (all rate constants are observed and at s^{-1}); b_2, diliganded closing rate constant; E_2, diliganded gating equilibrium constant ($= f_2/b_2$); ΔG_2, diliganded free energy change ($= -0.59 \ln E_2$); ΔG_0^{net}, net unliganded gating free energy (see Equation 1); ΔG_B, energy from the affinity change for ACh (see Equation 3). Values are mean ± S.E., *n* patches.

		Observed						
Mutant	bkg	f_2	b_2	E_2	ΔG_2	ΔG_0^{net}	ΔG_B	*n*
ϵProD2-A	B0+B4	5459 ± 118	3321 ± 55	1.60 ± 0.4	−0.3 ± 0.0	11.1 ± 0.3	−6.3 ± 0.3	2
-V	B0+B4	5111 ± 283	2920 ± 452	1.75 ± 0.5	−0.3 ± 0.1	9.6 ± 0.2	−4.8 ± 0.2	3
-S	B0+B4	2809 ± 134	3701 ± 121	0.83 ± 0.011	0.1 ± 0.0	10.8 ± 0.2	−5.5 ± 0.2	3
-C	B0+B4	1506 ± 47	2042 ± 26	0.74 ± 0.05	0.2 ± 0.0	9.5 ± 0.2	−4.2 ± 0.2	2
-T	B0+B4	2339 ± 331	3915 ± 602	0.6 ± 0.1	0.3 ± 0.1	9.7 ± 0.3	−4.3 ± 0.3	3
-D	B0+B4	834 ± 89	1760 ± 300	0.47 ± 0.08	0.4 ± 0.1			3
-K	B0+B4	561 ± 25	3491 ± 321	0.16 ± 0.02	1.1 ± 0.1	10.6 ± 0.2	−4.4 ± 0.2	3
-L	B0+B4	326 ± 30	4639 ± 420	0.07 ± 0.008	1.6 ± 0.1	8.5 ± 0.2	−1.9 ± 0.2	3
-Q	B0+B4	276 ± 27	4178 ± 499	0.07 ± 0.007	1.6 ± 0.1	9.5 ± 0.3	−2.8 ± 0.3	4
-Y	B0+B4	84 ± 8	1752 ± 279	0.05 ± 0.01	1.8 ± 0.1	7.8 ± 0.2	−0.9 ± 0.3	3
-H	B0+B5	216 ± 2	1159 ± 44	0.19 ± 0.03	1.0 ± 0.0	8.7 ± 0.2	−2.6 ± 0.2	4
-G	B0+B5	149 ± 21	2086 ± 294	0.07 ± 0.006	1.6 ± 0.1	9.6 ± 0.2	−2.9 ± 0.2	3
-R	B0+B5	211 ± 38	4175 ± 356	0.05 ± 0.009	1.8 ± 0.1	8.8 ± 0.2	−1.9 ± 0.3	4
δProD2-C	B0+B6	1522 ± 76	5850 ± 572	0.26 ± 0.01	0.8 ± 0.1	10.8 ± 0.2	−4.9 ± 0.2	3
-V	B0+B6	1366 ± 149	7387 ± 247	0.19 ± 0.02	1.0 ± 0.1	10.1 ± 0.2	−4.0 ± 0.2	3
-A	B0+B6	1080 ± 170	10,610 ± 935	0.1 ± 0.01	1.4 ± 0.1	10.3 ± 0.4	−3.9 ± 0.4	3
-Y	B0+B6	2163 ± 199	899 ± 185	2.6 ± 0.7	−0.6 ± 0.1	10.8 ± 0.2	−6.3 ± 0.3	3
-T	B0+B6	2451 ± 39	1271 ± 114	1.9 ± 0.14	−0.4 ± 0.1	11.4 ± 0.2	−6.7 ± 0.2	4
-H	B0+B6	1015 ± 29	943 ± 60	1.1 ± 0.03	−0.1 ± 0.0	10.9 ± 0.3	−5.9 ± 0.3	3
-S	B0+B6	225 ± 82	7449 ± 630	0.03 ± 0.01	2.1 ± 0.2	10.5 ± 0.2	−3.3 ± 0.3	4
-M	B0+B4	2572 ± 187	3061 ± 373	0.87 ± 0.07	0.1 ± 0.1			2
-L	B0+B6	289 ± 32	9696 ± 129	0.03 ± 0.003	2.1 ± 0.1	9.3 ± 0.3	−2.1 ± 0.3	3
-K	B0+B5	5409 ± 290	1414 ± 95	3.9 ± 0.4	−0.8 ± 0.1	7.6 ± 0.2	−3.3 ± 0.2	4
-Q	B0+B4	685 ± 126	1183 ± 23	0.58 ± 0.1	0.3 ± 0.1	11.0 ± 0.2	−5.5 ± 0.2	2
-G	B0+B4	432 ± 59	3239 ± 555	0.15 ± 0.04	1.1 ± 0.1	10.0 ± 0.3	−3.8 ± 0.4	3
-D	B0+B4	252 ± 12	1419 ± 115	0.19 ± 0.02	1.0 ± 0.1	10.5 ± 0.2	−4.4 ± 0.3	3
-R	B0+B5	269 ± 51	3007 ± 187	0.09 ± 0.003	1.4 ± 0.1	8.3 ± 0.3	−1.8 ± 0.3	4
ϵProD1-A	B0+B6	817 ± 34	6867 ± 365	0.12 ± 0.012	1.3			3
-F	B0+B6	1570 ± 314	4237 ± 446	0.37 ± 0.064	0.6			3
-L	B0+B6	1308 ± 132	6449 ± 554	0.20 ± 0.005	0.9			3
-R	B0+B6	1259 ± 60	3203 ± 64	0.39 ± 0.012	0.6			3
δProD1-A	B0+B6	1504 ± 39	5064 ± 205	0.3 ± 0.01	0.7			3
-F	B0+B6	2170 ± 457	3592 ± 824	0.6 ± 0.03	0.3			3
-L	B0+B6	1072 ± 162	3175 ± 149	0.3 ± 0.04	0.7			3
-R	B0+B6	1776 ± 175	4516 ± 443	0.4 ± 0.02	0.5			3

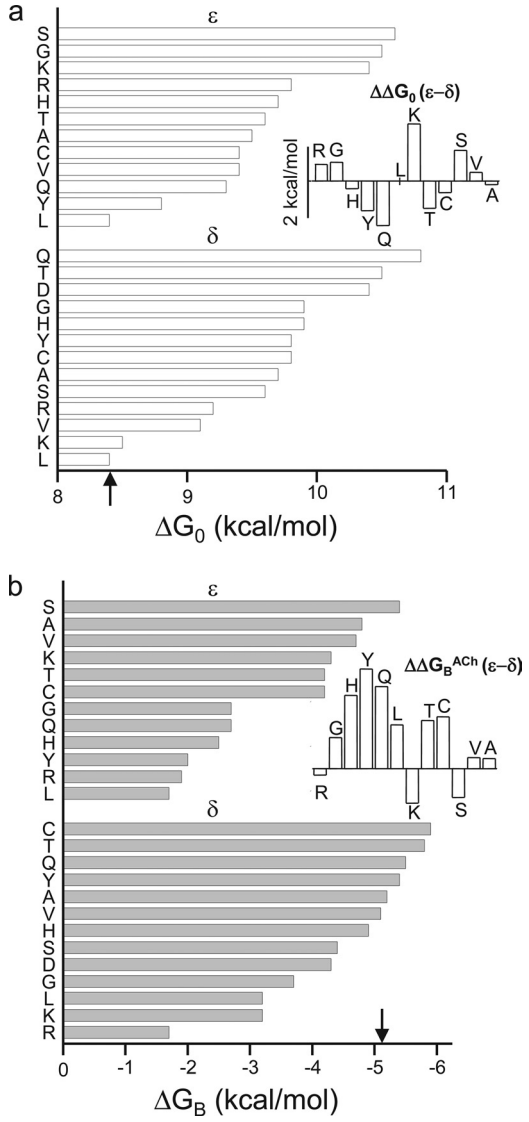

FIGURE 4. **Gating and binding energies of AChRs with ProD2 mutations.** *a*, energy of unliganded gating (ΔG_0). *Arrow* marks the WT value (+8.4 kcal/mol). In ϵ, the Ser mutation caused the largest loss in constitutive gating activity. *Inset*, differences in ΔG_0, ϵ *versus* δ. *b*, energy from the affinity change for ACh (ΔG_B^{ACh}). *Arrow* marks the WT value (−5.1 kcal/mol). In ϵ, the Leu mutation caused the largest reduction in binding energy. *Inset*, difference in ΔG_B^{ACh}, ϵ *versus* δ. Energy losses were in general larger in ϵ. $\Delta\Delta G_0$ and ΔG_B^{ACh} values for each ProD2 mutation are given in Tables 3 and 4.

were for Ser, Gly, and Lys substitutions (approximately +2 kcal/mol, which corresponds to an ~30-fold reduction in E_0). In δ, Gln, Thr, and Asp caused the largest increases in ΔG_0 (again, by approximately +2 kcal/mol). The *inset* of Fig. 4*a* compares the effect of mutations on ΔG_0 in the ϵ *versus* δ subunits. The biggest differences (>1.5 kcal/mol) were for Lys and Gln substitutions.

The effects of these and other ProD2 mutations on ΔG_B^{ACh} are shown in Fig. 4*b* (Table 4). In ϵ, large reductions in ΔG_B^{ACh} (>2 kcal/mol) were apparent with LRYHQG. In δ, the only large reduction was with Arg and Leu. The *inset* of Fig. 4*b* compares the effects of the various ProD2 mutations at the two binding sites with regard to ΔG_B^{ACh}. In most cases, the loss in energy from ACh was larger in the ϵ subunit compared with δ. However, the Arg substitution had nearly the same effect in ϵ and δ.

We also measured the effect of an Ala, Phe, or Arg mutation on E_2 (but not E_0) at ProD1, at both the α-ϵ- and α-δ-binding sites (Table 4). All of the mutations reduced E_2 but only to small extents (<7-fold).

Because we measured the opening and closing rate constants for each mutant, we could estimate a ϕ value for ProD2 in ϵ and δ (Fig. 5). ϕ is the slope of the rate *versus* equilibrium constant relationship (on a log-log scale) and gives the relative position in the gating isomerization at which the mutated side chain changes energy on a scale from 1 (early) to 0 (late). For diliganded gating, the ϕ value for ProD2 was high (≥0.9) in both subunits, although perhaps higher in α-ϵ compared with α-δ. This indicates that these prolines, like many other residues in the vicinity of the transmitter-binding sites, change energy relatively early, and nearly synchronously, in the opening isomerization when ACh is present (27). In the absence of agonists, the ProD2 residues at both ϵ and δ had slightly lower ϕ values, suggesting relatively later energy changes. Other binding site residues also show lower ϕ values for gating in the absence of agonists (24). Also, there was more scatter without agonists than with ACh present. Some of this variance may be from measurement noise, but some may also reflect the "catalytic" effects of the ProD2 mutations that are more apparent without ACh present.

Interactions between Residues—In the next series of experiments, we used mutant cycle analysis (28) to probe the extent to which the ProD2 residues in the ϵ and δ subunits interact energetically with each other and with two loop B glycine residues in the α subunit, αGlyB1 (αGly-147) and αGlyB2 (αGly-153) (see Fig. 1*c*). We chose these glycines because we were interested in the ProD2 backbone (rather than side chain) cross-subunit interactions and because they had been well characterized previously (21, 29). These two glycines have opposing effects on AChR activation, with mutations of αGlyB1 reducing and mutations of αGlyB2 increasing P_o (21). We measured both E_0 and E_2^{ACh} in Ser-Ser or Ala-Ala double mutant pairs, and we compared the calculated ΔG_0 (Table 5) and ΔG_B^{ACh} (Table 6) values with the sums for single Ser or Ala mutants. A positive interaction energy indicates that the effect of the mutant pair was greater than the sum of the energy changes generated by the individual mutations.

With regard to ϵProD2-δProD2 coupling, the unliganded ΔG_0 interaction energy was small (≤0.2 kcal/mol) for both Ser and Ala mutations. With ACh present, the ΔG_B^{ACh} interaction energy was slightly larger, ~+0.7 kcal/mol for the Ser-Ser pair and −0.4 kcal/mol for the Ala-Ala pair. These energies are close to our resolution limit, so we conclude that the two distant binding-site ProD2 residues interact weakly, if at all, regardless of whether or not ACh is present.

With regard to ProD2-αGlyB1 coupling, there was only a small ΔG_0 interaction at α-ϵ and none at all at α-δ, for both Ser and Ala pairs. With only water at the binding site, these residues on the primary and complementary sides of the binding pocket hardly communicate. However, the situation was different in the presence of ACh. The ΔG_B^{ACh} coupling energy was substantial at α-ϵ, where ProD2 and αGlyB1 interact by approxi-

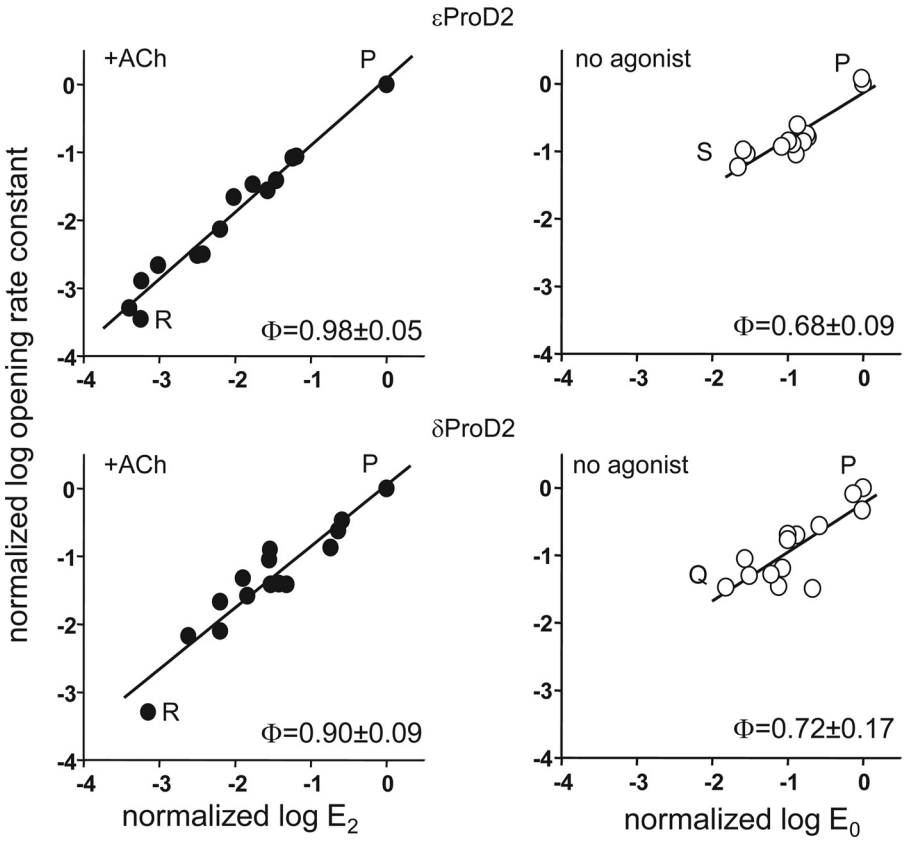

FIGURE 5. **Rate equilibrium plots for ProD2 mutants.** Φ is the slope of the log-log relationship and gives the relative position in the opening isomerization when ProD2 changes energy, on a scale from 1 (early) to 0 (late). With ACh present at the binding sites, both ϵProD2 and δProD2 change energy near the onset of channel opening (*solid circles*). With only water present at the binding sites, both prolines change energy somewhat later than with ACh present. Rate and equilibrium constants have been corrected for the background and are normalized to the WT value. Each symbol is the mean of ≥3 patches for one side chain substitution; Φ values are mean ± S.D.

TABLE 5

Interaction energies, ΔG_0

The abbreviations used are as follows: m1, mutant 1;m2, mutant 2; f_0, unliganded opening rate constant (all rate constants are observed (Obs) and at s^{-1}); b_0, unliganded closing rate constant; E_0, unliganded gating equilibrium constant ($=f_0/b_0$). Values are mean ± S.E. from ≥3 patches. All energies are in kcal/mol. $\Delta G_0^{m1+m2+bkg} = -0.59 \ln E_0^{obs}$; $\Delta G_0^{bkg} = -0.59 \ln E_0^{app}$) (see Table 1); $\Delta\Delta G_0^{dbl}$ (observed) $= \Delta G_0^{m1+m2+bkg} - \Delta G_0^{bkg}$; ΔG_0^{mut} predicted (Pred), sum of individual mutations ΔG_0 values (Table 3 or Ref. 21 for αGlyB1 and -2). Coupling energy, $\Delta\Delta G_0^{dbl}$(observed) − $\Delta\Delta G_0^{dbl}$(predicted).

m1	m2	bkg	f_0	b_0	E_0	$\Delta G_0^{m1+m2+bkg}$	ΔG_0^{bkg}	$\Delta\Delta G_0^{dbl}$ Obs	$\Delta\Delta G_0^{dbl}$ Pred	Coupling energy
ϵProD2-S	αGlyB1-S	B13	61 ± 6	3932 ± 476	0.016 ± 0.003	2.4	−0.3	2.75	3.4	−0.7
ϵProD2-A	αGlyB1-A	B13	177 ± 111	2608 ± 199	0.068 ± 0.001	1.6	−0.3	1.88	2.8	−0.9
δProD2-S	αGlyB1-S	B14	218 ± 22	7017 ± 138	0.031 ± 0.002	2.0	−0.3	2.39	2.4	0.0
δProD2-A	αGlyB1-A	B14	217 ± 16	7306 ± 372	0.030 ± 0.002	2.1	−0.3	2.41	2.4	0.0
δProD2-S	αGlyB2-S	B1	237 ± 32	2118 ± 78	0.112 ± 0.01	1.3	1.8	-0.51	−0.8	0.2
δProD2-A	αGlyB2-A	B1	307 ± -	1824 ± -	0.168 ± -	1.1	1.8	-0.75	−1.4	0.6
ϵProD2-S	δProD2-S	B4	53 ± 3	1476 ± 69	0.036 ± 0.003	2.0.	−1.4	3.39	3.5	−0.1
ϵProD2-A	δProD2-A	B4	273 ± 477	1110 ± 20	0.246 ± 0.04	0.8	−1.4	2.26	2.5	−0.2

mately +2.6 kcal/mol with Ser or Ala pairs. The degree of positive interaction energy at α-ϵ indicates that the fold-change in E_2^{ACh} for the mutant pair was ~30-fold larger than the product of the fold-changes for the individual mutations. The ΔG_B^{ACh} interaction energy was smaller at the α-δ interface.

We attempted to carry out similar analyses for interaction energies for ProD2-αGlyB2 interactions at both binding sites, but we could do so only at α-δ. At α-ϵ, the ProD2 + αGlyB2 pairs (both Ser and Ala) produced unliganded clusters having a wide distribution of open probabilities. This suggests that there is some interaction between these residues in the unliganded binding site, but a clear ΔG_0 value could not be estimated. The clusters for δProD2-αGlyB2 mutant pairs did not show this variance, and ΔG_0 and ΔG_B^{ACh} coupling estimates could be obtained (Tables 5 and 6). At α-δ, these two residues interact weakly, either with or without ACh present.

In summary, the only significant energy coupling we could measure was with regard to ΔG_B^{ACh}, between ϵProD2 and αGlyB1, and only when ACh is present.

Construction of One-site AChRs—In WT AChRs, each neurotransmitter molecule increases the gating equilibrium constant by ~6000-fold ($\Delta G_B^{ACh} = -5.1$ kcal/mol). However, with a ProD2-R mutation at either α-ϵ or α-δ, the gating equilibrium constant increases only by ~285-fold (average $\Delta G_B^{mut} = -3.4$ kcal/mol). We sought to use these substitutions to engineer

TABLE 6

Interaction energies, ΔG_B^{ACh}

The abbreviations used are as follows: m1, mutant 1;m2, mutant 2; f_2, diliganded opening rate constant (all rate constant are observed and at s^{-1}); b_2, diliganded closing rate constant; E_2, diliganded gating equilibrium constant ($= f_2/b_2$). Values are mean ± S.E. from ≥3 patches. All energies are in kcal/mol. $\Delta G_2^{m1+m2+bkg} = -0.59 \ln(E_2)$; ΔG_0^{net}, net unliganded free energy (see Equation 1). $\Delta G_{B1} + \Delta G_{B2}$ (observed) $= \Delta G_2^{m1+m2+bkg} - \Delta G_0^{net}$. $\Delta G_{B1} + \Delta G_{B2}$ (predicted) $= \Delta G_{B1}^{WT} + \Delta\Delta G_{B1}^{m1} + \Delta\Delta G_{B1}^{m2} + \Delta\Delta G_{B2}^{m2}$ (see Equation 5 and "Experimental Procedures"). The ΔG_B^{m2} values are from either Table 4 (ProD2) or see Ref. 21 (αGlyB1 and -2). Coupling energy, $\Delta G_{B1}+\Delta G_{B2}$ (observed) − $\Delta G_{B1} + \Delta G_{B2}$ (predicted).

m1	M2	bkg	f_2	b_2	E_2	$\Delta G_2^{m1+m2+bkg}$	ΔG_0^{net}	$\Delta G_{B1}+\Delta G_{B2}$ Obs	$\Delta G_{B1}+\Delta G_{B2}$ Pred	Coupling energy
ϵProD2-S	αGlyB1-S	B5+B0	35 ± 1	6597 ± 157	0.005 ± 0.0001	3.1	7.4	−4.4	−7.1	**2.7**
ϵProD2-A	αGlyB1-A	B5+B0	25 ± 5	5286 ± 686	0.005 ± 0.002	3.1	6.6	−3.4	−6.0	**2.6**
δProD2-S	αGlyB1-S	B11+B0	385 ± 17	3274 ± 284	0.12 ± 0.016	1.3	6.5	−5.2	−5.9	0.7
δProD2-A	αGlyB1-A	B11	57 ± 13	2181 ± 164	0.026 ± 0.004	2.2	7.1	−5.0	−6.3	1.4
δProD2-S	αGlyB2-S	B6+B0	2068 ± 83	4908 ± 186	0.42 ± 0.01	0.5	10.0	−9.5	−8.3	−1.1
δProD2-A	αGlyB2-A	B12	47 ± 1	7474 ± 848	0.006 ± 0.0005	3.0	12.8	−9.8	-10.3	0.5
ϵProD2-S	δProD2-S	B8+B0	2000 ± 197	983 ± 112	2.04 ± 0.014	−0.4	8.7	−9.1	−9.8	0.7
ϵProD2-A	δProD2-A	B10+B0	249 ± 18	1155 ± 120	0.22 ± 0.013	0.9	11.2	−10.3	−9.9	−0.4

AChRs having only one functional binding site, either α-ϵ (by using the δProD2-R knock-out) or α-δ (by using the ϵProD2-R knock-out). Although we did not measure the resting affinity of the Arg mutants, it is likely that these substitutions also increases K_d^{ACh}, further lowering activation by ACh.

Fig. 6*a* shows single-channel activity in 500 μM ACh (~3 times $K_d^{ACh, WT}$) in WT, single-site, and double-site knock-outs. As expected, activity was greatly reduced when either of the two binding sites was incapacitated by the Arg substitution, and there was almost no activity in the double mutant combination. The infrequent openings apparent in the double knock-out can be attributed to the residual ΔG_B^{ACh} energies at the two binding sites.

In the single-site knock-outs, the activity generated by the lone WT-binding site was insufficient to cause openings to occur in clusters. To allow cluster analysis, we added a distant gain-of-function background mutation that decreased ΔG_0 but had no effect on either ΔG_B^{ACh} or K_d^{ACh}, either αS269I in M2 ($\Delta\Delta G_0 = -2.8$ kcal/mol (18) or αP272A in the M2-M3 linker ($\Delta\Delta G_0 = -3.2$ kcal/mol (30)). With either background, the gating activity of the double knock-out in 500 μM ACh was too low to generate clusters (data not shown), perhaps because binding was reduced by the two Arg substitutions.

Fig. 6*b* shows clusters of openings in 500 μM ACh from AChRs having just one functional WT transmitter-binding site (αS269I background). The mono-liganded shut and open intracluster interval durations apparent with ACh activating only the α-δ site (top) were described by single exponentials, so a clear estimate of E_1^{ACh} and ΔG_1^{ACh} could be obtained (+1.9 kcal/mol). Using Equation 1, we calculated a ΔG_0^{net} for each construct. For αS269I + ϵProD2R (−100 mV), $\Delta G_0^{net} = +8.4 - 2.8 + 1.4 = +7.0$ kcal/mol. From the relationship $\Delta G_{B2}^{ACh} = \Delta G_1^{ACh} - \Delta G_0^{net}$, we now calculate that the agonist energy from the functional α-δ site was $\Delta G_{B2}^{ACh} = +1.9 - 7.0 = -5.1$ kcal/mol (Table 7).

The mono-liganded shut and open intracluster interval durations apparent with ACh activating only the α-ϵ site were each described by two exponentials, with both backgrounds (Fig. 6*b*, *bottom panel*). We used the inverse time constant of the predominant component to estimate E_1^{ACh} and $\Delta G_1^{ACh} = +1.8$ kcal/mol. Using the method described above, we estimate that with the αS269I background the agonist energy from the functional α-ϵ site was −4.7 kcal/mol.

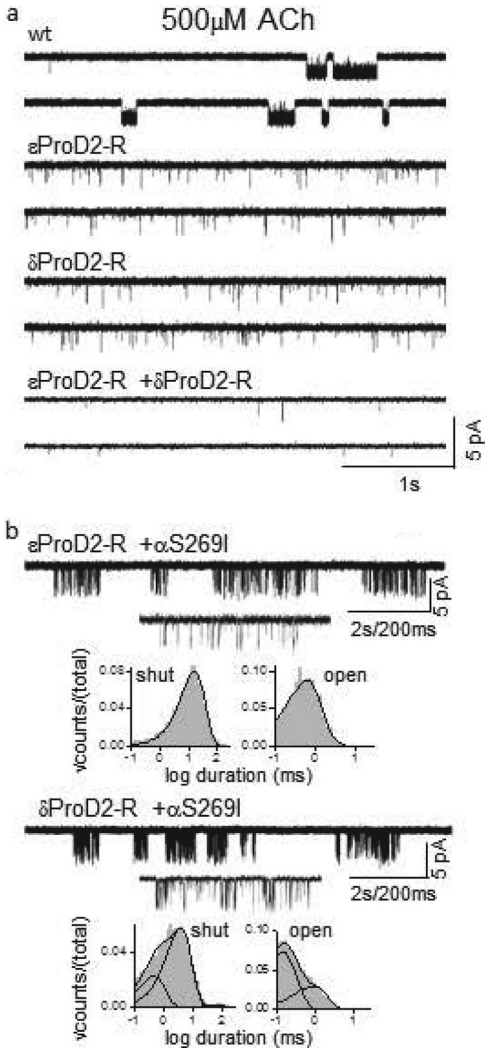

FIGURE 6. **Engineering AChRs having only one functional transmitter-binding site.** *a,* single-channel currents from AChRs having two (*top*), one (*middle traces*), or zero (*bottom*) WT transmitter-binding sites. The sites were made nonfunctional by using either a ϵProD2-R or δProD2-R knock-out mutation. *b,* gating properties of one-site AChRs. Each *panel* shows a low time resolution trace, a single cluster, and interval duration histograms (500 μM ACh, −100 mV). In addition to the ProD2-R mutation, a background mutation (αS269I) was added that decreased ΔG_0 to enhance cluster formation. From the gating equilibrium constants, $\Delta G_B^{ACh} = -5.1$ and −4.7 kcal/mol at the α-δ and α-ϵ transmitter-binding sites.

TABLE 7

Mono-ligand gating rate and equilibrium (ACh)

The abbreviations used are as follows: m1, mutant 1;m2, mutant 2; f_2, diliganded opening rate constant (all rate constant are observed and at s^{-1}); b_2, diliganded closing rate constant; E_2, diliganded gating equilibrium constant ($= f_2/b_2$). Values are mean ± S.E. from ≥3 patches. All energies are in kcal/mol. $\Delta G_2^{m1+m2+bkg} = -0.59 \ln(E_2)$; ΔG_0^{net}, net unliganded free energy (see Equation 1). $\Delta G_{B1} + \Delta G_{B2}$ (observed) $= \Delta G_2^{m1+m2+bkg} - \Delta G_0^{net}$. $\Delta G_{B1} + \Delta G_{B2}$ (predicted) $= \Delta G_{B1}^{WT} + \Delta\Delta G_{B1}^{m1} + \Delta\Delta G_{B1}^{m2} + \Delta\Delta G_{B2}^{m2}$ (see Equation 5 and see "Experimental Procedures"). The ΔG_B^{m2} values are from either Table 4 (ProD2) or Ref. 21 (αGlyB1 and -2). Coupling energy, $\Delta G_{B1} + \Delta G_{B2}$ (observed) − $\Delta G_{B1} + \Delta G_{B2}$ (predicted).

Construct	f_1	b_1	E_1	ΔG_1	ΔG_0^{net}	ΔG_B	n
ϵProD2-R + αS269I	76 ± 10	1765 ± 48	0.043 ± 0.008	1.9	7.0	−5.1	3
ϵProD2-R + αP272A	91 ± 8	1549 ± 72	0.059 ± 0.008	1.7	6.6	−4.9	3
δProD2-R + αS269I	377 ± 28	8078 ± 74	0.047 ± 0.004	1.8	6.5	−4.7	3
δProD2-R + αP272A	397 ± 21	6172 ± 82	0.064 ± 0.005	1.6	6.1	−4.5	2

Using the same approaches and the αP272A background mutation, we estimate that ΔG_B^{ACh} is −4.9 and −4.5 kcal/mol at the WT α-δ and α-ϵ transmitter-binding sites. The agreement between the ΔG_B^{ACh} values using two backgrounds is evidence that the αS269I and αP272A mutations only change ΔG_0 (and not ΔG_B^{ACh}) and do not interact energetically with either ProD2-R.

DISCUSSION

CMS Mutation—The CMS mutation (ϵProD2-L) has a similar functional effect in mouse AChRs as in human AChRs, which is to reduce both the resting affinity for ACh and the diliganded gating equilibrium constant. Because we measured the effect of this mutation on ΔG_0, we could also calculate its effect on ΔG_{B1}^{ACh}, which is the energy provided by the neurotransmitter for gating at the α-ϵ-binding site. The reduction in this energy, from −5.1 to −1.9 kcal/mol, was substantial. In effect, the CMS mutation turns the AChR from a two-site to a one-site receptor. The primary effect of many other CMS mutations is to decrease ΔG_0 (31). The ϵProD2-L is an exception to this pattern because it has no effect on ΔG_0 but a large one on ΔG_B^{ACh}.

Because we measured both K_d^{ACh} (≈510 μM) and the affinity ratio (≈19) for the CMS mutation, we could calculate, using the thermodynamic cycle (Fig. 2*a*), the equilibrium dissociation constant for ACh binding to the high affinity open channel conformation of the α-ϵ transmitter binding site. The estimate, $J_{d1}^{ACh} = 27$ μM, is 1000-fold higher than the WT value of 28 nM (32). With regard to mechanism, the large reduction in the affinity of the O-conformation of the α-ϵ transmitter-binding site, a +4.1 kcal/mol loss in energy, is by far the main effect of the CMS mutation with regard to AChR activation.

Recently, evidence was presented suggesting that low and high affinity binding of agonists occurs by an integrated process called "catch-and-hold" (26). The results with ϵProD2-L indicate that this substitution has a much smaller effect on the low affinity "catch" phase (~3-fold) than on low to high affinity "hold" (~1000-fold). This indicates that the energy change at ϵProD2 occurs late in catch-and-hold, because most of the energy (structure) change takes place when the binding site switches from low to high affinity. Apparently, with Leu at this position, ACh can bind reasonably well with a low affinity, but a high affinity cannot be established.

The leucine substitution of ProD2 at the α-δ-binding site had a much smaller effect on ΔG_B^{ACh}, and mutation of ProD1 at either binding site had very little effect. Of the side chains we examined, only the ProD2-R substitutions reduced ΔG_B^{ACh} to similar extents as the leucine, at both binding sites.

Transmitter-binding Sites—So far, eight positions in the vicinity of the AChR-binding sites have been probed in detail regarding the effects of mutations on ΔG_0 and ΔG_B^{ACh} (see Fig. 1*c*). These include four aromatic amino acids in the α subunit αTyr-93 (TyrA), αTrp-149 (TrpB), αTyr-190 (TyrC1), and αTyr-198 (TyrC2), two glycines in loop B αGly-147 (GlyB1) and αGly-153 (GlyB2), a tryptophan on the complementary D surface ϵTrp-55/δTrp-57 (TrpD), and now ϵ/δProD2 (21, 24, 27, 33). In WT AChRs, most of the ΔG_B^{ACh} energy comes from an "aromatic triad" composed of αTrp-149, αTyr-190, and αTyr-198 (27).

At α-ϵ, AChRs having the WT Pro or the CMS mutation Leu have the same ΔG_0 value (+8.4 kcal/mol). All other substitutions increased ΔG_0, with the largest increase (biggest loss of function) being for Ser, Gly, and Lys (Fig. 3*a*). Overall, the range of intrinsic gating energy values, smallest (WT) to largest (δProD2-Q), was <2.5 kcal/mol, which indicates that as a rule the ϵProD2 side chain does not change energy to a great extent when the unliganded binding site switches its conformation in gating. This energy range is similar to the ΔG_0 range energies of some other residues at the binding site for which unliganded gating has been measured (TyrC1, TyrC2, GlyB1, TrpD, and TyrA). So far, only GlyB2 and TrpB show more substantial (≥4 kcal/mol) unliganded gating range energies (21, 24).

Large side chains can adopt alternate rotamers and, without structures, it is difficult to speculate about the structural basis of the energetic consequences of such substitutions. Although we tested many different side chains at ϵProD2, below we consider the effects on ΔG_B^{ACh} for only the small amino acids GASV. Of these, at α-ϵ only the Gly substitution had a large effect on ΔG_B^{ACh}, decreasing the energy from the transmitter by +2.5 kcal/mol. The other three small side chains hardly affected this energy (<+0.3 kcal/mol). The ϵProD2-Gly change in ΔG_B^{ACh} is large and approximately equivalent to that observed by replacing the central loop B tryptophan (αTrp-149) with an Ala (+2.3 kcal/mol (27)). So far, for the small side chain substitutions only the mutation TyrC2-A has been shown to have a greater effect on ΔG_B^{ACh} than ϵProD2-G. Recall that the Gly substitution also had a large effect on ΔG_0, suggesting that the gating conformational change at ϵProD2 may be similar in unliganded and liganded conditions.

The energy coupling estimates obtained by using mutant cycle analyses were informative. There was little or no ΔG_0 coupling between ϵProD2 and αGlyB1 in the absence of ACh, but with ACh present a strong ΔG_B^{ACh} interaction was apparent (+2.7 kcal/mol). Although this coupling estimate does not distinguish between the two mutated αGlyB1 residues, we

assume that the interaction was exclusively between ϵProD2 and the αGlyB1 at the α-ϵ site. It appears that these two residues on different sides of the binding pocket act in concert (are effectively "cross-linked") when the binding site switches from low to high affinity, but only when ACh is present. It is noteworthy that the αGlyB1-A mutation alone decreases substantially the energy from ACh (by +2.4 kcal/mol; see Ref. 21). So far, αGlyB1 and ϵProD2 are the only binding site elements outside of the aromatic triad where GASV mutations have been found to change significantly ΔG_B^{ACh}.

The mutation and coupling studies together indicate that ϵProD2 plays an important role in AChR gating. (i) ϵProD2 changes energy mainly in the low to high affinity conformational switch. (ii) Of the small amino acids, only a Gly substitution causes a large reduction in ΔG_B^{ACh}. (iii) The energy changes of ϵProD2 and αGlyB1 are tightly coupled when ACh is present. Our interpretation of these results is that there is a concerted strain in the backbones at the ϵProD2 and αGlyB1 positions when the liganded binding site switches from low to high affinity. A Pro does not appear to be critical for maintaining the appropriate backbone architecture on the complementary surface because Ala, Ser, and Val all have WT-like ΔG_B^{ACh} values. We speculate that when ACh is in the binding pocket, during the affinity switch a force, perhaps initiated by the movement of loop B residue αGlyB1, is applied across subunits to the ProD2 backbone. With a Gly here, the binding pocket is deformed (relative to the WT) so as to reduce the high affinity of the O conformation and, hence, the energy for gating arising from ACh.

At α-δ, the effects of ProD2 mutations were more muted than at α-ϵ. The ΔG_0 and ΔG_B^{ACh} energy changes with a Gly were about half those at α-ϵ. Also, there was less apparent δProD2-αGlyB1 coupling with ACh present. This highlights that the two AChR binding sites are different even though they supply about the same ΔG_B^{ACh} energies for gating. Further evidence is that the YQH substitutions had large effects at α-ϵ but only small effects at α-δ. The reduction in agonist energy consequent to these larger amino acid substitutions (including the CMS mutation) may not be from a change in the ϵ/δ backbone but rather from unfavorable interactions of the larger side chains with other structural elements at the binding site. Still, the ProD2-G substitution at α-δ had the largest effect on ΔG_B^{ACh} among the small side chains, so perhaps the above hypothesis of a backbone strain here applies to α-δ as well as α-ϵ.

The loss of agonist energy is probably not from unfavorable direct interactions between the ProD2 backbone and the neurotransmitter. Rather, it may be that a puckering of the complementary subunit backbone in the low to high affinity rearrangement affects J_d^{ACh} indirectly, for example by generating an overall shape of the pocket that is sub-optimal for establishing a high affinity from one or more elements of the aromatic triad. Our understanding of the AChR transmitter-binding sites is in its infancy. It will be interesting to learn the magnitudes of the ligand energy arising from the aromatic triad in the ϵProD2-G mutant, and whether ϵProD2 is coupled energetically to other residues at the α-ϵ-binding site.

Although the ϵProD2-G substitution had a large effect on both ΔG_0 and ΔG_B^{ACh}, the quantitative effects of the substitutions were different with water *versus* ACh present in the binding site. For example, the Ser substitution reduced unliganded gating but had little effect on ΔG_B^{ACh}, with the opposite result for the Leu substitution. This suggests that the conformational changes at the binding site are not identical without *versus* with ACh present. The lower ϕ values for unliganded gating, and the absence of energy coupling between ProD2 and αGlyB1 in water-only, support this hypothesis. The thermodynamic cycle is useful for estimating energies, but it is only an approximation. Although most residue energy changes in many regions of the AChR are approximately the same without *versus* with ligands (3, 34), it appears that the structural changes of the few residues that provide ΔG_B^{ACh} energy are different in the two conditions.

Engineering—Using the single-site knock-outs (ϵ-δ), we confirmed the previous finding that each binding site provides approximately the same ΔG_B^{ACh} energy, but our measurements are not sufficiently precise to allow us to distinguish −5.1 (α-δ) *versus* −4.7 kcal/mol (α-ϵ) (values obtained using the αS269I background). The sources of this energy, and the net binding energy from agonists other than ACh and choline, have not been measured at the two sites separately. However, the observation that there is little if any communication between the ProD2 side chains α-ϵ and α-δ suggests that the binding sites operate almost independently.

The knock-outs were not perfect because there was a residual ΔG_B^{ACh} energy (approximately −1.7 kcal/mol) with the Arg substitution. However, we have demonstrated that by using [ACh] that causes a high occupancy probability of the WT-binding sites, it is possible to study AChRs that have only one functional binding site, either α-ϵ or α-δ. This ability to engineer single-site AChRs may prove valuable in probing further the differences between the two transmitter-binding sites.

Acknowledgments—We thank M. Merritt, M. Shero, and M. Teeling for technical assistance.

REFERENCES

1. Jadey, S. V., Purohit, P., Bruhova, I., Gregg, T. M., and Auerbach, A. (2011) Design and control of acetylcholine receptor conformational change. *Proc. Natl. Acad. Sci. U.S.A.* **108,** 4328–4333
2. Nayak, T. K., Purohit, P. G., and Auerbach, A. (2012) The intrinsic energy of the gating isomerization of a neuromuscular acetylcholine receptor channel. *J. Gen. Physiol.* **139,** 349–358
3. Purohit, P., and Auerbach, A. (2009) Unliganded gating of acetylcholine receptor channels. *Proc. Natl. Acad. Sci. U.S.A.* **106,** 115–120
4. Auerbach, A. (2010) The gating isomerization of neuromuscular acetylcholine receptors. *J. Physiol.* **588,** 573–586
5. Lester, H. A., Dibas, M. I., Dahan, D. S., Leite, J. F., and Dougherty, D. A. (2004) Cys-loop receptors: new twists and turns. *Trends Neurosci.* **27,** 329–336
6. Sine, S. M., and Engel, A. G. (2006) Recent advances in Cys-loop receptor structure and function. *Nature* **440,** 448–455
7. Celie, P. H., van Rossum-Fikkert, S. E., van Dijk, W. J., Brejc, K., Smit, A. B., and Sixma, T. K. (2004) Nicotine and carbamylcholine binding to nicotinic acetylcholine receptors as studied in AChBP crystal structures. *Neuron* **41,** 907–914
8. Ohno, K., Wang, H. L., Milone, M., Bren, N., Brengman, J. M., Nakano, S., Quiram, P., Pruitt, J. N., Sine, S. M., and Engel, A. G. (1996) Congenital

myasthenic syndrome caused by decreased agonist binding affinity due to a mutation in the acetylcholine receptor ϵ subunit. *Neuron* **17,** 157–170
9. Peter, C., Korngreen, A., and Witzemann, V. (2005) Mutation of single murine acetylcholine receptor subunits reveals differential contribution of P121 to acetylcholine binding and channel opening. *Pflugers Arch.* **450,** 178–184
10. Qin, F. (2004) Restoration of single-channel currents using the segmental *k*-means method based on hidden Markov modeling. *Biophys. J.* **86,** 1488–1501
11. Qin, F., Auerbach, A., and Sachs, F. (1997) Maximum likelihood estimation of aggregated Markov processes. *Proc. Biol. Sci.* **264,** 375–383
12. Qin, F., Auerbach, A., and Sachs, F. (1996) Estimating single-channel kinetic parameters from idealized patch-clamp data containing missed events. *Biophys. J.* **70,** 264–280
13. Auerbach, A. (2013) The energy and work of a ligand-gated ion channel. *J. Mol. Biol.*, in press
14. Karlin, A. (1967) On the application of "a plausible model" of allosteric proteins to the receptor for acetylcholine. *J. Theor. Biol.* **16,** 306–320
15. Monod, J., Wyman, J., and Changeux, J. P. (1965) On the nature of allosteric transitions: a plausible model. *J. Mol. Biol.* **12,** 88–118
16. Chakrapani, S., Bailey, T. D., and Auerbach, A. (2003) The role of loop 5 in acetylcholine receptor channel gating. *J. Gen. Physiol.* **122,** 521–539
17. Mitra, A., Bailey, T. D., and Auerbach, A. L. (2004) Structural dynamics of the M4 transmembrane segment during acetylcholine receptor gating. *Structure* **12,** 1909–1918
18. Mitra, A., Cymes, G. D., and Auerbach, A. (2005) Dynamics of the acetylcholine receptor pore at the gating transition state. *Proc. Natl. Acad. Sci. U.S.A.* **102,** 15069–15074
19. Purohit, P., and Auerbach, A. (2007) Acetylcholine receptor gating: movement in the α-subunit extracellular domain. *J. Gen. Physiol.* **130,** 569–579
20. Jha, A., and Auerbach, A. (2010) Acetylcholine receptor channels activated by a single agonist molecule. *Biophys. J.* **98,** 1840–1846
21. Purohit, P., and Auerbach, A. (2011) Glycine hinges with opposing actions at the acetylcholine receptor-channel transmitter-binding site. *Mol. Pharmacol.* **79,** 351–359
22. Auerbach, A. (2005) Gating of acetylcholine receptor channels: Brownian motion across a broad transition state. *Proc. Natl. Acad. Sci. U.S.A.* **102,** 1408–1412
23. Lape, R., Colquhoun, D., and Sivilotti, L. G. (2008) On the nature of partial agonism in the nicotinic receptor superfamily. *Nature* **454,** 722–727
24. Purohit, P., and Auerbach, A. (2010) Energetics of gating at the apo-acetylcholine receptor transmitter-binding site. *J. Gen. Physiol.* **135,** 321–331
25. Cadugan, D. J., and Auerbach, A. (2007) Conformational dynamics of the αM3 transmembrane helix during acetylcholine receptor channel gating. *Biophys. J.* **93,** 859–865
26. Jadey, S., and Auerbach, A. (2012) An integrated catch-and-hold mechanism activates nicotinic acetylcholine receptors. *J. Gen. Physiol.* **140,** 17–28
27. Purohit, P., Bruhova, I., and Auerbach, A. (2012) Sources of energy for gating by neurotransmitters in acetylcholine receptor channels. *Proc. Natl. Acad. Sci. U.S.A.* **109,** 9384–9389
28. Horovitz, A., and Fersht, A. R. (1990) Strategy for analysing the co-operativity of intramolecular interactions in peptides and proteins. *J. Mol. Biol.* **214,** 613–617
29. Jadey, S., Purohit, P., and Auerbach, A. (2013) Action of nicotine and analogs on acetylcholine receptors having mutations of transmitter-binding site residue αG153. *J. Gen. Physiol.* **141,** 95–104
30. Jha, A., Cadugan, D. J., Purohit, P., and Auerbach, A. (2007) Acetylcholine receptor gating at extracellular transmembrane domain interface: the Cys-loop and M2-M3 linker. *J. Gen. Physiol.* **130,** 547–558
31. Zhou, M., Engel, A. G., and Auerbach, A. (1999) Serum choline activates mutant acetylcholine receptors that cause slow channel congenital myasthenic syndromes. *Proc. Natl. Acad. Sci. U.S.A.* **96,** 10466–10471
32. Grosman, C., and Auerbach, A. (2001) The dissociation of acetylcholine from open nicotinic receptor channels. *Proc. Natl. Acad. Sci. U.S.A.* **98,** 14102–14107
33. Bafna, P. A., Jha, A., and Auerbach, A. (2009) Aromatic residues ϵTrp-55 and δTrp-57 and the activation of acetylcholine receptor channels. *J. Biol. Chem.* **284,** 8582–8588
34. Gupta, S., and Auerbach, A. (2011) Mapping heat exchange in an allosteric protein. *Biophys. J.* **100,** 904–911
35. Unwin, N. (2005) Refined structure of the nicotinic acetylcholine receptor at 4A resolution. *J. Mol. Biol.* **346,** 967–989